Nonlinear Dyn (2007) 47:193–217
DOI 10.1007/s11071-006-9067-3

ORIGINAL ARTICLE

Hybrid (numerical-experimental) modeling of complex structures with linear and nonlinear components

D. Giagopulos · S. Natsiavas

Received: 31 October 2005 / Accepted: 25 January 2006 / Published online: 3 November 2006

Abstract The present work investigates the performance of two systematic methodologies leading to hybrid modeling of complex mechanical systems. This is done by applying numerical methods in determining the equations of motion of some of the substructures of large order mechanical systems, while the dynamic characteristics of the remaining components are determined through the application of appropriate experimental procedures. In their simplest version, the models examined are assumed to possess linear characteristics. For such systems, it is possible to apply several hybrid methodologies. Here, the first of the methods selected is performed in the frequency domain, while the second method has its roots and foundation in time domain analysis. Originally, the accuracy and effectiveness of these methodologies is illustrated by numerical results obtained for two complex mechanical models, where the equations of motion of each substructure are first set up by applying the finite element method. Then, the equations of motion of the complete system are derived and their dimension is reduced substantially, so that the new model is sufficiently accurate up to a prespecified level of forcing frequencies. The formulation is developed in a general way, so that application of other methods, including experimental techniques, is equally valid. This is actually performed in the final part of this study, where experimental results are employed in conjunction with numerical results in order to predict the dynamic response of a mechanical structure possessing a linear substructure with high modal density, supported on four substructures with strongly nonlinear characteristics.

Keywords Dimension reduction · Hybrid modeling · Large scale structures · Nonlinear supports · Substructuring

1. Introduction

The rapid advances taking place over the last three decades in the area of producing more effective electronic devices caused significant and ever increasing advantages in terms of computation speed and memory capacity of current electronic computers. This in turn has resulted in an equally great progress in many areas of engineering and technological interest. Specifically, the developments in the areas of computer hardware and software caused a flourishing in the fields of improving or even inventing new, more accurate and more effective experimental and numerical methodologies, with large engineering importance. As a consequence, substantial advances have been achieved in attacking and solving challenging problems in many scientific areas, including the general area of experimental and computational dynamics of systems with nonlinear characteristics (e.g., [1–4]).

D. Giagopulos · S. Natsiavas (✉)
Department of Mechanical Engineering, Aristotle University, 541 24 Thessaloniki, Greece
e-mail: natsiava@auth.gr

The main objective of the present work is to demonstrate the advantages of applying appropriate hybrid methodologies in order to study the dynamics of complex mechanical structures in an accurate and effective way. Development and application of such methodologies is based on a drastic reduction in the dimensions of the systems examined and is a necessary step in order to explain and improve the dynamic behavior of contemporary mechanical systems. More specifically, apart from increasing the computational and experimental efficiency and speed, the reduction of the system order makes amenable the application of several numerical or experimental techniques for determining the dynamic response of complex systems, which are applicable and efficient for linear or low order nonlinear dynamical systems [3–8].

In particular, two substructuring methods are applied, both of which start by splitting the original system into a number of components. Then, depending on the nature of the system, some of its components are modeled numerically, while the remaining components are modeled experimentally. The first methodology applied has its roots in a frequency domain formulation. Such approaches are particularly suitable for systems possessing linear characteristics, which are measured experimentally, or for systems involving components with frequency dependent properties [8–13]. However, these methods are usually limited by the fact that they are applicable to systems with linear and time invariant characteristics only. Therefore, when the system nonlinearities are activated and affect the response beyond a certain level, their predictions become inaccurate. For this reason, a second hybrid method is applied here, which is based on a classical component mode synthesis method and is founded on theoretical developments in the time domain [12–15].

The effectiveness and accuracy of the methods applied is first demonstrated by presenting numerical results obtained for two complex mechanical structures. They both result in a drastic reduction of the dimensions and help the efforts towards a systematic and comprehensive study of the dynamics exhibited by large order linear mechanical models [4, 12]. Then, the same methodologies are applied in an actual hybrid context. Specifically, the dynamic response of a frame structure, designed to exhibit a relatively large modal density and to involve nonlinear elements, is investigated. The composite structure is split into a frame substructure, which possesses linear properties determined through application of a finite element analysis, plus four supporting substructures, whose characteristics are strongly nonlinear and are measured experimentally.

The organization of this paper is as follows. First, the basic theoretical ingredients of the two hybrid methodologies applied are briefly presented in the following section. In the third section, these methodologies are applied to involved finite element mechanical models of a geared rotor-bearing system and a ground vehicle. The numerical results presented establish the accuracy and effectiveness of both methodologies for linear systems by comparison of results obtained for the reduced and the corresponding complete dynamical models. Moreover, emphasis is placed on examining the residual flexibility effects. In the fourth section, these methods are applied in order to experimentally study the dynamics of a frame structure, whose frame substructure is linear but exhibits high modal density, while its four supporting substructures are characterized by nonlinear behavior. A summary of the highlights is presented in the final section.

2. Methods of analysis

Current industrial design requirements lead frequently to the examination of large scale mechanical models [4, 12]. Typically, the equations of motion of these models are first set up by applying classical finite element techniques. As the order of these models increases, the existing numerical and experimental methodologies for a systematic determination of their dynamic response become inefficient to apply. The situation becomes worse when the system includes components with nonlinear action. Therefore, there is a need for the development, improvement and application of new suitable methodologies for investigating dynamics of large scale mechanical models in a systematic and efficient way. Traditionally, in the area of structural dynamics this is done by first employing methodologies that reduce the dimensions of the original system, by applying methods either in the frequency domain [8–11] or in the time domain [12–15]. Next, the basic philosophy of two such representative reduction methods is presented briefly in the following two subsections.

2.1. A frequency domain reduction method

The class of reduction methods with analytical foundation lying on a frequency domain approach is based

on an accurate (analytical or experimental) evaluation of the matrix with the Frequency Response Functions (FRFs) of the system. For a system with linear properties and general damping, this matrix appears in the form

$$H(\omega) = \left(-\omega^2 M + i\omega C + K \right)^{-1}.$$

However, when evaluation of elements of this matrix is required at several frequency values, the above definition demands extensive computations, which for large order systems are prohibitive. These calculations can be performed in an alternative and equivalent way, by first solving the complex eigenvalue problem

$$(\lambda_r^2 M + \lambda_r C + K)\underline{\hat{x}}_r = \underline{0},$$

which is also associated with extensive computations [12]. On the other hand, the assumption that the structural component examined is classically damped is in most cases satisfactory and appealing. In such cases, the FRF matrix can be obtained in the form

$$H(\omega) = \sum_{r=1}^{N} \frac{\underline{\varphi}_r \underline{\varphi}_r^T}{\omega_r^2 - \omega^2 + 2i\omega\omega_r\zeta_r},$$

where the quantities ω_r and $\underline{\varphi}_r$ represent the solution of the much easier to solve real eigenproblem

$$\left(K - \omega_r^2 M\right)\underline{\varphi}_r = \underline{0},$$

while ζ_r is the damping ratio of the r-th mode. Moreover, for cases with frequency content $\omega \ll \omega_{k+1}$, this matrix can be represented by the simpler form

$$H(\omega) = \sum_{r=1}^{k} \frac{\underline{\varphi}_r \underline{\varphi}_r^T}{\omega_r^2 - \omega^2 + 2i\omega\omega_r\zeta_r} + H_R(\omega), \tag{1}$$

where the high frequency residue appears in the form

$$H_R(\omega) = \sum_{r=k+1}^{N} \frac{\underline{\varphi}_r \underline{\varphi}_r^T}{\omega_r^2 - \omega^2 + 2i\omega\omega_r\zeta_r} \approx H_{R1} + i\omega H_{R2} + \omega^2 H_{R3} \tag{2}$$

and can be computed conveniently [12, 16].

Once the FRF matrix of a linear system is known, its response can be determined in the frequency domain by the well-known formula

$$\underline{x}(\omega) = H(\omega)\underline{f}(\omega). \tag{3}$$

In particular, if a system is composed of component A and component B, the response of component A is first expressed in the form

$$\begin{pmatrix} \underline{x}_i^A \\ \underline{x}_b^A \end{pmatrix} = \begin{bmatrix} H_{ii}^A & H_{ib}^A \\ H_{bi}^A & H_{bb}^A \end{bmatrix} \begin{pmatrix} \underline{f}_i^A \\ \underline{f}_b^A \end{pmatrix},$$

where the vectors $\underline{x}_i^A$ and $\underline{x}_b^A$ include the internal and the boundary degrees of freedom of component A, respectively. In addition, the components $\underline{f}_i^A$ and $\underline{f}_b^A$ of the forcing vector have an analogous meaning. If a similar partitioning is also employed for the degrees of freedom of component B, after imposing the appropriate compatibility conditions for the displacements and the forces at the common nodes, the response of the composite system is determined from Equation (3), with

$$\underline{x} = \begin{pmatrix} \underline{x}_i^A \\ \underline{x}_i^B \\ \underline{x}_b \end{pmatrix}, \ \underline{x}_b = \underline{x}_b^A = \underline{x}_b^B, \ \underline{f} = \begin{pmatrix} \underline{f}_i^A \\ \underline{f}_i^B \\ \underline{f}_b^A + \underline{f}_b^B \end{pmatrix},$$

and composite FRF matrix

$$H = \begin{bmatrix} H_{ii}^A & H_{ib}^A & 0 \\ H_{bi}^A & H_{bb}^A & 0 \\ 0 & 0 & H_{ii}^B \end{bmatrix} - \begin{bmatrix} H_{ib}^A \\ H_{bb}^A \\ -H_{ib}^B \end{bmatrix} \times \left[H_{bb}^A + H_{bb}^B \right]^{-1} \begin{bmatrix} H_{ib}^A \\ H_{bb}^A \\ -H_{ib}^B \end{bmatrix}^T. \tag{4}$$

When the system examined possesses more than two components, the above process needs to be repeated until all components are successively included in the formulation. Alternatively, it can be generalized so that the synthesis is performed at one step. Moreover, this technique is especially useful in hybrid formulations. For instance, in problems involving fluid-structure interaction (e.g., in acoustics of structures) for some of the components of the system, Equation (3) may relate pressure loads to pressure coordinates [8]. Finally,

the FRFs for some of the system components may be determined experimentally. In such cases, special attention should be devoted to overcoming numerical difficulties associated with the part of Equation (4) that needs inversion. However, the most important drawback of the methodology is that its applicability is limited to linear systems, possessing equations of motion with constant coefficients only.

2.2. A time domain reduction method

For simplicity, consider again a mechanical model consisting of subsystems A and B. Moreover, let the equations of motion for subsystem A be derived by any appropriate method and put in the following classical form

$$\hat{M}_A \underline{\ddot{x}}_A + \hat{C}_A \underline{\dot{x}}_A + \hat{K}_A \underline{x}_A = \underline{\hat{f}}_A(t), \tag{5}$$

where $\hat{M}_A$, $\hat{C}_A$ and $\hat{K}_A$ are the mass, damping and stiffness matrix of the subsystem, respectively, while the vector $\underline{f}_A(t)$ represents the external forcing. For a typical model, the order of these equations may be quite large. However, for a given level of forcing frequencies it is possible to reduce significantly the number of degrees of freedom, without sacrificing the accuracy in the numerical results, by applying standard component mode synthesis methods [4–6, 12]. In particular, this can be achieved through a coordinate transformation with form

$$\underline{x}_A = \Psi_A \underline{q}_A. \tag{6}$$

The transformation matrix Ψ_A includes an appropriately chosen set of normal modes, depending on the accuracy required in the response frequency range examined, plus the static correction modes of component A. For large order systems, even the calculation of the columns of this matrix is quite challenging and special methods need to be applied. However, by employing this transformation the original set of Equations (5) can be replaced by a considerably smaller set of equations, expressed in terms of the new generalized coordinates $\underline{q}_A$. More specifically, application of the Ritz transformation (6) into the original set of Equations (5) yields the smaller set

$$M_A \underline{\ddot{q}}_A + C_A \underline{\dot{q}}_A + K_A \underline{q}_A = \underline{f}_A(t), \tag{7}$$

where

$$M_A = \Psi_A^T \hat{M}_A \Psi_A,\ C_A = \Psi_A^T \hat{C}_A \Psi_A,$$
$$K_A = \Psi_A^T \hat{K}_A \Psi_A \quad \text{and} \quad \underline{f}_A = \Psi_A^T \underline{\hat{f}}_A.$$

In addition, the vector of unknowns can be split in the form

$$\underline{q}_A = \left(\underline{p}_A^T \ \underline{x}_b^T \right)^T,$$

where the vector $\underline{p}_A$ includes coordinates related to the response of internal degrees of freedom of component A, while the vector $\underline{x}_b$ includes the boundary points of component A.

Next, similar sets of equations of motion are obtained for substructure B. Namely, following the same steps as those for component A, the equations of motion are first set up in the form

$$M_B \underline{\ddot{q}}_B + C_B \underline{\dot{q}}_B + K_B \underline{q}_B = \underline{f}_B(t), \tag{8}$$

with

$$\underline{q}_B = \left(\underline{p}_B^T \ \underline{x}_b^T \right)^T.$$

Then, a proper combination of Equations (7) and (8) leads to the equations of motion of the composite system in the classical form

$$M \underline{\ddot{q}} + C \underline{\dot{q}} + K \underline{q} = \underline{f}(t), \tag{9}$$

with

$$\underline{q} = \left(\underline{p}_A^T \ \underline{p}_B^T \ \underline{x}_b^T \right)^T.$$

For instance, the stiffness matrix of the composite system can be obtained by considering the potential energy of the system and its components in the form

$$V = V_A + V_B \Rightarrow \frac{1}{2} \underline{q}^T K \underline{q} = \frac{1}{2} \underline{q}_A^T K_A \underline{q}_A + \frac{1}{2} \underline{q}_B^T K_B \underline{q}_B.$$

Likewise, the mass matrix of the composite system is obtained by considering the corresponding kinetic energies, while the forcing vector is determined by considering the virtual work [4, 12]. Finally, the contribution of more components is added in a similar manner.

In closing this subsection, it is worth pointing out that this method presents certain advantages over the alternative frequency domain method outlined in the previous subsection. Specifically, the time domain method is applicable even when the system examined involves general damping properties or nonlinear components. In such cases, the corresponding degrees of freedom are included in the set of boundary degrees of freedom and the equations of motion are put in the form

$$M\underline{\ddot{q}} + C\underline{\dot{q}} + K\underline{q} + \underline{p}(\underline{x}_b, \underline{\dot{x}}_b) = \underline{f}(t). \tag{10}$$

Typically, the number of equations of motion of the reduced system is substantially smaller than the dimension of the original system. Therefore, the reduction of the model order makes possible the application of methodologies, which are suitable for low order dynamical systems [3].

3. Numerical results

In order to assess their accuracy and effectiveness for large order systems, the methodologies presented in the previous section were first applied to two example mechanical models. The results obtained are included in the following two subsections.

3.1. Application to a gear-pair system

The first example mechanical system is shown in Fig. 1. This model represents a gear-pair system supported on deformable bearings. Component A consists of the driving gear and its bearing subsystem, while component B consists of the driven gear and its bearing subsystem. In both cases, the gear is geometrically discretized by solid (hexahedral) finite elements, while the bearing is represented by an equivalent spring-damper system with linear characteristics. Finally, the engagement action of the two gears is modeled through the use of appropriate rigid body elements [17]. As a result, the equations of motion of the dynamical system examined are linear and can eventually be put in the matrix form (9). The final model possesses 143,103 degrees of freedom (32,616 associated with the driving and 110,487 with the driven gear subsystem). Then, a reduced model was selected, so that the system response is accurate for

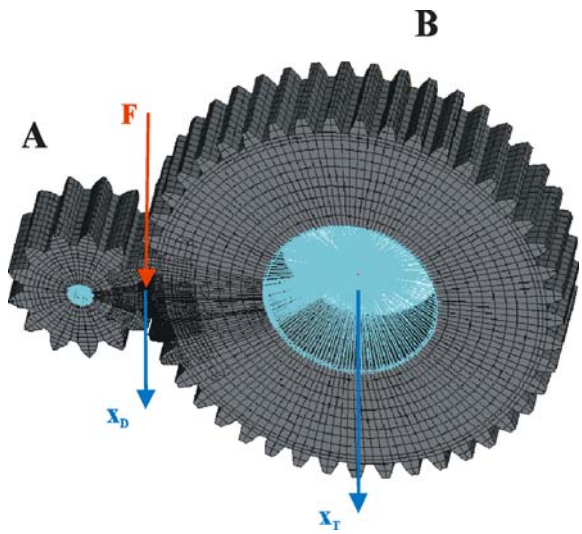

Fig. 1 Finite element model of a gear-pair system

frequencies up to about 10,000 Hz. This led to a new model with only 40 degrees of freedom. In particular, besides the normal modes of the two gears (6 for the small and 30 for the large gear), the set of boundary degrees of freedom includes two degrees of freedom at the support of the bearings and two degrees of freedom at the gear engagement position.

The first set of numerical results is shown in Fig 2. In particular, Fig. 2a presents the drive point inertance, obtained for an applied load and a measured acceleration component at a point along the line of action of the two gears. First, the FRF-based substructuring method described in subsection 2.1 was applied. Each of the two substructures was assumed to possess classical damping. In particular, a typical value of 0.01 was selected as the damping ratio for each linear mode. The continuous line corresponds to the exact values, obtained by running the complete model. Likewise, the dashed line was obtained by applying Equation (4) without including the static correction. Finally, the dotted line corresponds to results obtained by applying Equation (4) after including the static correction. Direct comparison indicates that the results obtained after including the static correction terms virtually coincide with the results of the original model for frequencies up to 3,500 Hz. Similar conclusions can also be drawn by inspecting Fig. 2b, which presents similar results for the transfer inertance function obtained for a load applied at a location along the line of action of the two gears and an acceleration component

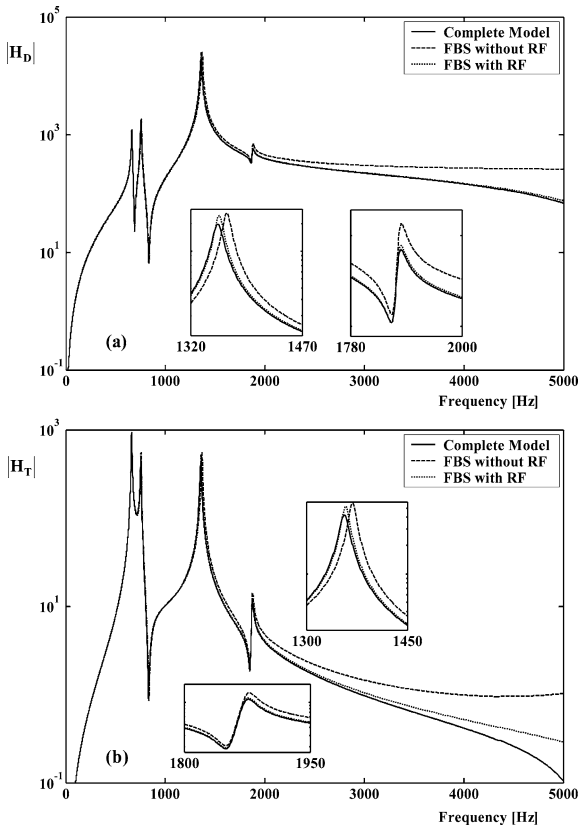

Fig. 2 Results obtained for the geared system by applying the FRF-based substructuring method and classical damping: (a) drive point inertance function; (b) transfer inertance function

measured at the bearing of the driven gear. Moreover, here it is more obvious that outside the prespecified frequency range the deviation between the predictions of the reduced and the complete model becomes more noticeable. These results demonstrate the accuracy of the method applied. The method becomes even more attractive when taking into account the considerable reduction in the amount of time required in the computations.

Next, Table 1 shows the four lowest natural frequencies obtained for the system examined, which are the frequencies appearing in the diagrams of Fig. 2. Specifically, the second column includes the natural frequencies of the complete model, the third column indicates the natural frequencies obtained for the model resulting by applying the FRF-based substructuring (FBS) method, while the last column includes similar results obtained by the component mode synthesis (CMS) method. Obviously, the results confirm the accuracy in computing the values of the natural frequencies of the composite system within the frequency range of interest.

Table 1 Natural frequencies of the gear-pair model examined.

ω_r(Hz)	Complete Model	FBS	CMS
1	662	662	662
2	754	754	754
3	1356	1358	1357
4	1873	1873	1873

In the sequel, the calculations were repeated for the same model and the same points by applying the component mode synthesis method described in subsection 2.2, instead. Moreover, in this case, each substructure was assumed to possess Rayleigh damping, with a damping ratio of 0.01 in the first and the fifth linear mode [12]. The results obtained are presented in Figs. 3a and 3b and the conclusions are quite similar to those drawn by inspecting Figs. 2a and 2b, respectively. In addition, the response amplitudes are different close to resonances, especially at the higher frequency modes, where the Rayleigh method assigns higher damping ratios.

3.2. Application to a ground vehicle

The same methodologies were subsequently applied to an involved mechanical model of a ground vehicle. This model is shown in Fig. 4 and includes the body-in-white structural component, together with the front and the rear suspension subsystems plus the wheels. The equations of motion were first set up and put in matrix form (9) by applying the finite element method [17]. Here, the attention is focused on ride vehicle behavior and the external excitation is assumed to result from road irregularities. The geometry of the vehicle structure is discretized by (rectangular and triangular) shell elements mainly and the total number of degrees of freedom of the resulting model is about 524,000.

The main objective here is to perform a direct comparison in the accuracy of the two reduction methodologies considered. For this reason, the equations of motion of the vehicle model were first linearized around its static equilibrium position. At the beginning, the calculations were performed by applying the frequency domain method described in subsection 2.1. The same calculations were then repeated by applying the time domain method outlined in Section 2.2. In both cases,

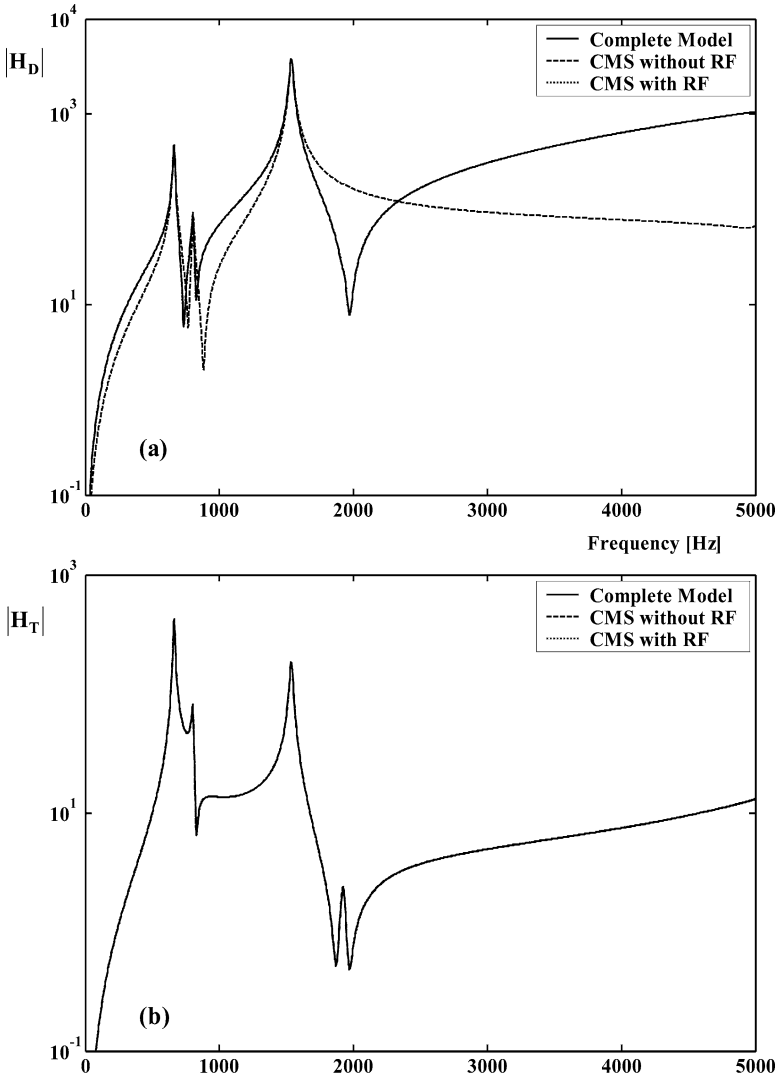

Fig. 3 Results obtained for the geared system by applying the component mode synthesis method and Rayleigh damping: (a) drive point inertance function; (b) transfer inertance function

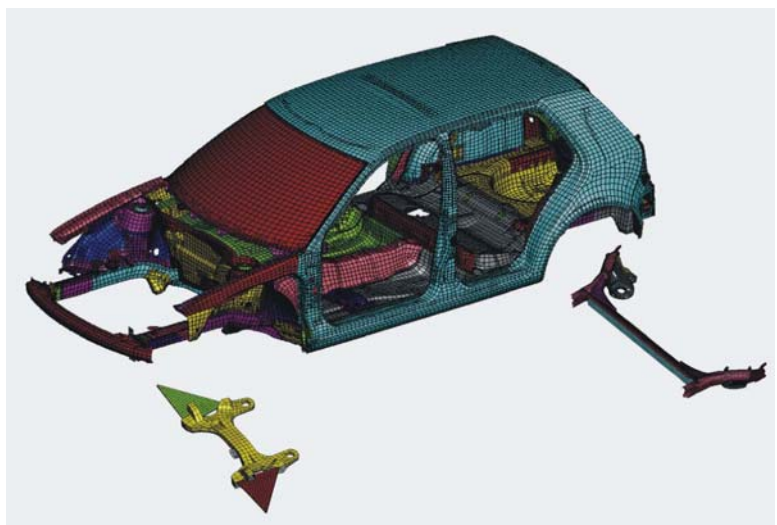

Fig. 4 Finite element model of a ground vehicle: body plus front and rear suspensions

each of the three substructures shown in Fig. 4 was assumed to possess classical damping, with a damping ratio of 0.01 in each linear mode. Moreover, the reduced model was selected so that the system response is sufficiently accurate for frequencies up to at least 100 Hz. This necessitated the inclusion of 274 degrees of freedom associated with the corresponding normal modes of the structural components. These were added to the set of boundary degrees of freedom, including 26 degrees of freedom at the front suspension and 16 degrees of freedom at the rear suspension.

First, a comparison of results obtained from the complete and the reduced models was performed once again, just like for the gear-pair system examined before. Then, a direct comparison was performed between results obtained by the frequency domain and the time domain method for the same mechanical model. For instance, Figs. 5a and 5b include results obtained by determining the drive point and the transfer inertance function for an excitation point at the front left wheel and measurement point at the same position or at a point near the driver's position, respectively. The continuous lines in these figures were determined by applying the CMS method, while the dashed lines were obtained by applying the FBS method. Both cases were run with the reduced model and after including the contribution of the static correction. Direct comparison indicates that the results obtained by the two reduction methodologies virtually coincide within the specified frequency range of interest. Some small deviations are justified partly by the different way of including the residual flexibility effects and partly by the loss of accuracy associated with the matrix inversion required in Equation (4), when applying the FBS method.

4. Experimental results

The numerical results presented in the previous section provided sufficient confidence for the accuracy and performance of the dimension reduction methodologies presented in the second section, at least when they are applied to complex mechanical models with linear properties. In the sequel, results obtained by the same methodologies are presented, determined within a hybrid formulation framework, where some components of a composite system are modeled numerically while the important properties of the others are measured experimentally. For this purpose, these methodologies were initially applied to simple beam structures, since a direct comparison with analytical results was possible in that case [18]. Then, a more involved experimental device was selected and set up, simulating the response of a ground vehicle. More specifically, the selected frame structure comprises a frame substructure with predominantly linear response and high modal density plus four supporting substructures with strongly nonlinear action. Here, results referring to the second experimental device only will be presented. At the beginning, a description of the experimental set up and the way of measuring its parameters is presented in the following subsection. Finally, experimental results are presented for the response of the model tested, by first employing the dimension reduction methodologies of Section 2.

4.1. Experimental set up and parameter identification

First, Fig. 6 shows a picture with an overview of the experimental set up. In particular, the mechanical system tested consists of a frame substructure, simulating the frame of a vehicle, supported on four identical substructures. These supporting substructures consist of a lower set of discrete spring and damper units connected to a concentrated (lighter color) mass, simulating the wheel subsystems, as well as of an upper set of a discrete spring and damper units connected to the frame and simulating the action of the vehicle suspension. In the last figure, the most important instruments used for performing the experimental measurements are also shown. In brief, the main experimental instruments used include the following:

- accelerometers Piezobeam 8632C10, 8690C10, 8634B5 and K-beam 8312A2 from Kistler Instrumente AG,
- load cell type 9712B250 from Kistler Instrumente AG,
- impulse force hammer type 9724A5000 from Kistler Instrumente AG,
- electromagnetic shaker ET-140 and amplifier PA-141 from Labworks Instrument,
- analog to digital converter cards, PCI-4551, PCI-4552 Dynamic signal acquisition and PCI-6552 E-series from National Instruments and

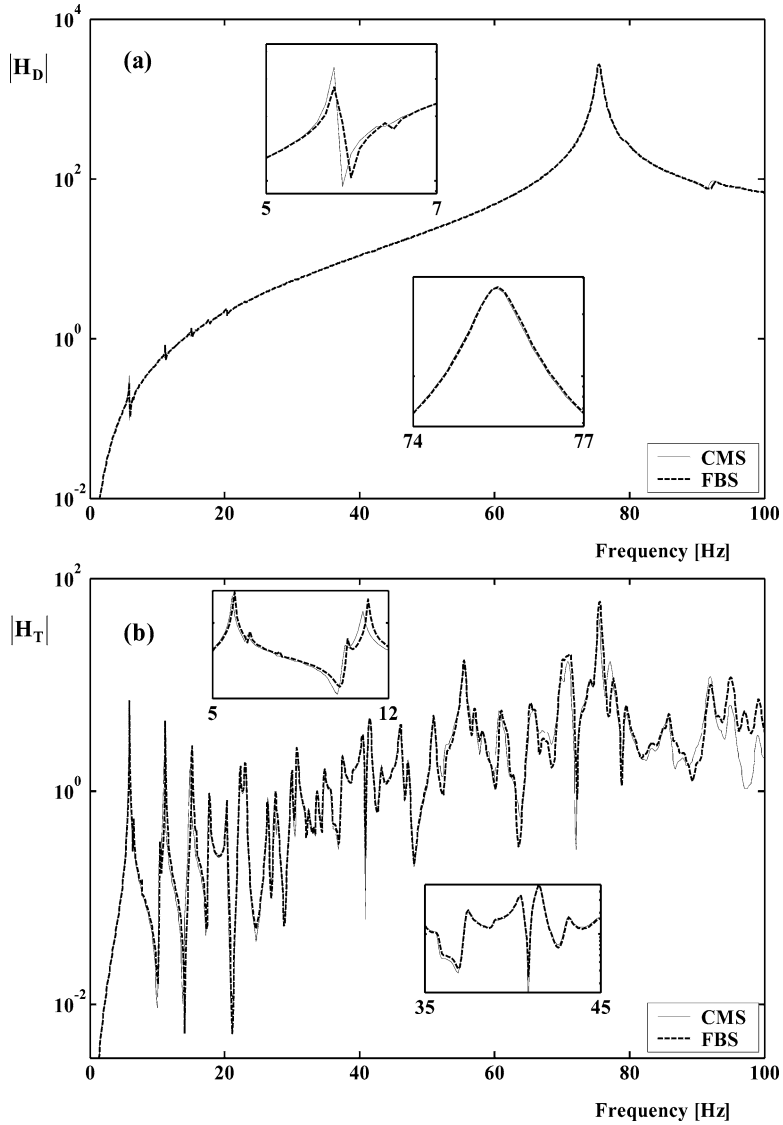

Fig. 5 Comparison of results obtained for the vehicle model by the FRF-based and the CMS substructuring method: (a) drive point inertance function; (b) transfer inertance function

- data acquisition and signal processing software Labview 7.0.

Next, Fig. 7 presents more details and the geometrical dimensions of the frame subsystem alone. The frame substructure is made of steel with Young's modulus $E = 2.1 \times 10^{11}$ N/m^2, Poisson's ratio $\nu = 0.3$ and density $\rho = 7850\,\mathrm{kg/m^3}$. Moreover, the measurement points indicated by 1–4 correspond to connection points between the frame and its supporting structures, while the other measurement points shown coincide with characteristic points of the frame. Finally, point E denotes the point where the electromagnetic shaker is applied.

First, all the necessary elements of the FRF matrix required for determining the response of the frame substructure were determined by imposing impulsive loading. The characteristics of this loading were selected appropriately, so that it causes sufficient excitation to all the linear modes of the frame with natural frequencies up to about 300 Hz. On the other hand, the sampling frequency was chosen as 512 Hz, so that harmonic components of the signals measured with frequencies below 250 Hz are picked up accurately. Moreover, the duration of each measurement was longer than about 30 sec, so that the system comes to a complete stop practically after imposing the excitation. The experimental data

Fig. 6 Experimental set up and instrumentation of the structure tested

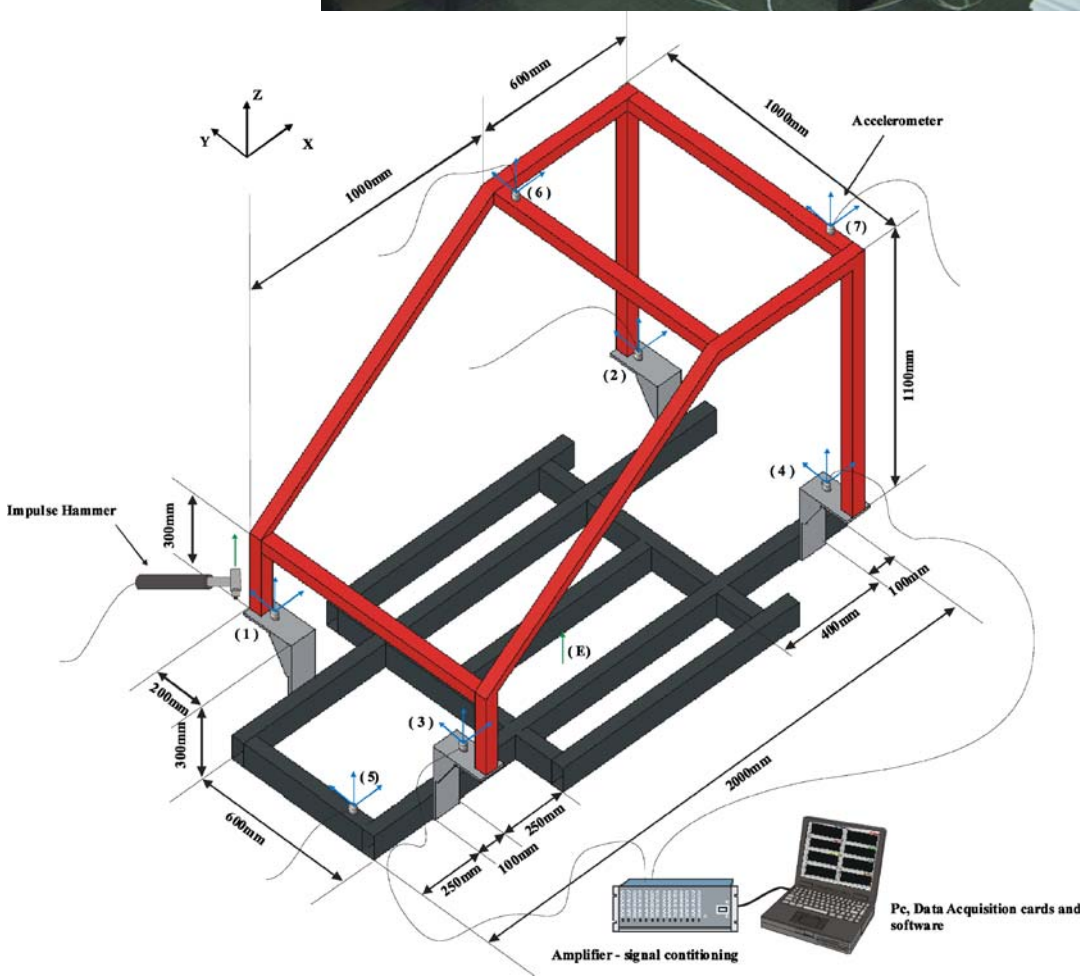

Fig. 7 Dimensions and measurement points of the frame substructure

Table 2 Natural frequencies of the frame substructure

ω_r [Hz]	Peak-Amplitude	MODE-ID	RFPM	FEM	Error (%)
1	23.81	23.72	23.71	23.25	2.00
2	41.97	41.64	41.57	41.35	0.53
3	42.37	42.14	42.15	42.11	0.10
4	47.81	47.89	47.88	48.90	2.08
5	58.11	58.17	58.16	59.01	1.43
6	68.70	68.69	68.69	67.53	1.71
7	69.18	69.14	69.14	69.95	1.15
8	79.14	79.04	79.39	81.78	2.91
9	85.65	86.25	86.25	86.18	0.08
10	100.02	100.37	100.36	102.38	1.96
11	102.58	102.42	102.40	106.28	3.65
12	110.37	110.29	110.28	109.81	0.44
13	115.07	114.90	114.89	114.81	0.07
14	123.83	123.54	123.50	124.11	0.48
15	127.57	127.40	127.40	129.54	1.65
16	131.80	132.28	132.28	134.67	1.78
17	134.51	134.79	134.76	136.52	1.29
18	138.11	138.82	138.77	142.39	2.54
19	147.82	148.27	148.27	149.63	0.90
20	164.51	164.15	164.15	162.37	1.10

collected were then passed through an antialising filter in order to avoid frequency overlapping and cut parasitic frequencies in the measured signal due to mechanical or electronic noise. For instance, Fig. 8 shows the magnitude of two typical elements of the FRF matrix before (continuous line) and after (dashed line) application of the Welsh's smoothing method in conjunction with an appropriate Hanning's window [18]. In particular, Fig. 8a depicts the diagonal element of the FRF matrix corresponding to measuring the vertical acceleration at point 5 (as shown in Fig. 7) due to a vertical excitation applied at the same point. Likewise, Fig. 8b shows the non-diagonal element corresponding to vertical excitation applied at the same point but measuring the vertical acceleration at point 3 of the frame.

Table 3 Damping ratios of the frame substructure

ζ_r	Peak-Amplitude	MODE-ID	RFPM
1	0.003512	0.003523	0.003147
2	0.006445	0.003871	0.004161
3	0.003132	0.002949	0.002813
4	0.002612	0.002635	0.002315
5	0.003755	0.002878	0.002604
6	0.003459	0.003364	0.003008
7	0.003989	0.003061	0.002712
8	0.006488	0.006851	0.006790
9	0.005522	0.008198	0.006817
10	0.002859	0.002033	0.001807
11	0.002492	0.001869	0.001834
12	0.002408	0.001617	0.001446
13	0.002225	0.001692	0.001460
14	0.002011	0.001403	0.001289
15	0.001185	0.001243	0.001108
16	0.002407	0.001711	0.001526
17	0.003618	0.002906	0.002575
18	0.002460	0.001535	0.001328
19	0.002388	0.001622	0.001430
20	0.002098	0.001407	0.001278

Based on the measured FRF functions, the natural frequencies and the damping ratios of the frame substructure were first estimated, by applying the classical method of peak amplitude [9, 12]. As an outcome of this, the second column of Table 2 presents the values of the lowest 20 natural frequencies determined, while the corresponding damping ratios are included in the second column of Table 3. Among other things, the results verify the high modal density of the frame substructure.

Using the results obtained by the approximate method of maximum magnitude of the transfer functions as a basis, more involved and accurate methods were applied subsequently. First, a method developed by Beck was applied [19]. As a result, the third column of Table 2 presents the lowest 20 natural frequencies, while the third column of Table 3 includes the corresponding damping ratios, evaluated after application of Beck's method. On the other hand, another

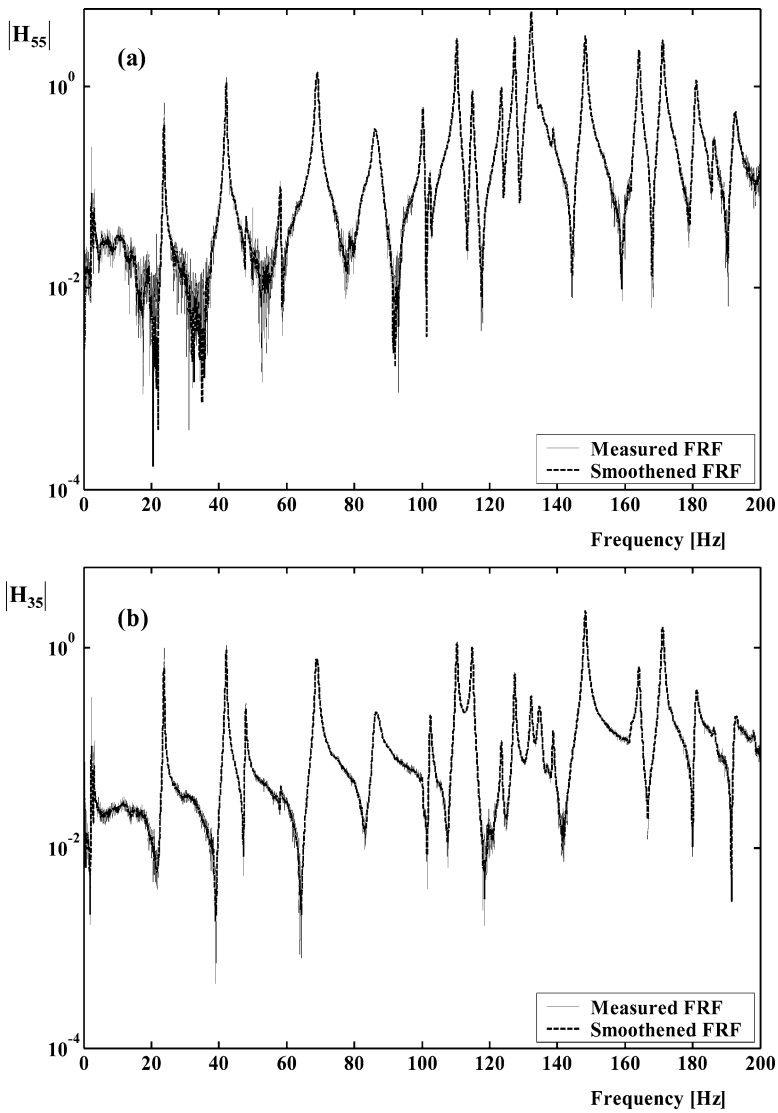

Fig. 8 Results from an experimental determination of typical elements of the FRF matrix for the frame substructure before (continuous line) and after (dashed line) smoothing: (a) point inertance function; (b) transfer inertance function

commonly applied method, the "Rational Fraction Polynomial Method" (RFPM) does not require initial estimation of the modal parameters. This method has certain attractive merits, especially for systems with high modal density, like the system under consideration. Briefly, in order to achieve better numerical accuracy, the whole frequency range is first split into smaller intervals and the modal parameters are then determined over these smaller frequency ranges [20]. In particular, application of RFPM to the system examined led to values of the lowest 20 natural frequencies and the corresponding damping ratios, which are put in the fourth columns of Tables 2 and 3, respectively.

Next, the experimental results obtained for the frame substructure were also compared with results obtained by modeling the same structure with finite elements. Specifically, the frame was divided into a number of shell (quadrilateral) and solid (mostly hexahedral and a few pentahedral) finite elements. The resulting model possesses about 45 thousand degrees of freedom. First, the values of the lowest 20 natural frequencies obtained by the finite element analysis are included in the fifth column of Table 2 presents. Moreover, the last column of the same table compares these frequencies with the corresponding frequencies obtained from the experimental data after application of RFPM. Obviously, the errors determined are sufiiciently low. Finally, the

results of Fig. 9 are presented in an effort to further verify and illustrate the accuracy of the methods applied. For instance, the dashed line of Fig. 9a represents the magnitude of the same element of the FRF matrix as that shown in Fig. 8a, obtained from the finite element model as a function of the forcing frequency. On the other hand, the continuous line represents the magnitude of the same quantity, as was determined experimentally. Likewise, Fig. 9b compares the time history of the vertical acceleration signals measured at point 3, due to an impulsive excitation imposed vertically at point 5. In particular, the continuous line represents the signal that was determined experimentally, while the dashed line represents the corresponding signal that was reconstructed analytically, after improving the experimental predictions through application of Beck's method.

From the experimental data collected, it was confirmed that the action of the frame substructure is predominantly linear. On the other hand, tests performed on trying to identify the parameters of the four supporting subsystems revealed that they exhibit strongly nonlinear characteristics. To investigate this further, the elements of the supporting units were disassembled and tested separately. First, Fig. 10a presents graphically the necessary details of the experimental device that was set up for measuring the stiffness and damping properties of the supports, while Fig. 10b shows the equivalent mechanical model.

The experimental process was applied separately for both the lower and the upper spring and damper units of the supporting substructures and can be briefly described as follows. First, the system shown in Fig. 10 is excited by harmonic forcing through the electromagnetic shaker up until it reaches a periodic steady state response. When this happens, both the history of the acceleration and the forcing signals are recorded at each forcing frequency. Some characteristic results obtained in this manner are presented in the following figures.

Next, Fig. 11a presents the transmissibility function of the system tested, obtained experimentally for three different forcing levels. Specifically, this function is defined as the ratio of the root mean square value of the acceleration to the root mean square value of the forcing signal measured at each forcing frequency. The continuous, dashed and dotted lines correspond to the smallest, intermediate and largest forcing amplitude, respectively. Clearly, the deviations observed between the forcing levels indicate that the system examined possesses nonlinear properties. Moreover, neither the applied forcing is harmonic, especially within the frequency range below $\omega = 10$ Hz. To illustrate this, Fig. 11b shows two periods of the actual excitation force applied for the same three excitation levels in obtaining the results of Fig. 11a, which were recorder at a fundamental forcing frequency of $\omega = 4$ Hz.

In particular, several forms of the restoring and damping forces, say f_r and f_d, respectively, were tried for modeling the action of the supports and compared with the experimental results. First, the classic linear dependence of the restoring force on the displacement and of the damping forces on the velocity of the support unit was assumed. However, critical comparison with the experimental results demonstrated that the outcome was unacceptable in terms of accuracy. After several tries, it was eventually found that the best form of the restoring forces is the one were they remain virtually in a linear relation with the extension of the spring, namely

$$f_r(x) = kx, \tag{11}$$

while the damping force was best approximated by the following formula

$$f_d(\dot{x}) = c_1\dot{x} + \frac{c_2\dot{x}}{c_3 + |\dot{x}|}. \tag{12}$$

As usual, the linear term in the last expression is related to internal friction at the support, while the nonlinear part is related to the existence and activation of dry friction. More specifically, in the limit $c_3 \to 0$, the second term in the right hand side of Equation (12) represents energy dissipation action corresponding to dry friction. On the other side, in the limit $c_3 \to \infty$, this term represents classical viscous action and can actually be absorbed in the first term.

The value of the constants appearing in the assumed forms of the restoring and damping forces of the supports, like the coefficients k, c_1, c_2 and c_3 in Equations (11) and (12), was determined by applying appropriate identification methodologies [21, 22]. For instance, Fig. 12 presents optimum values obtained for the coefficients k and c_1 of the linear terms in the restoring and damping forces. In all cases, two sets of results are presented, obtained for two different forcing levels, corresponding to the intermediate and higher forcing used in obtaining the results

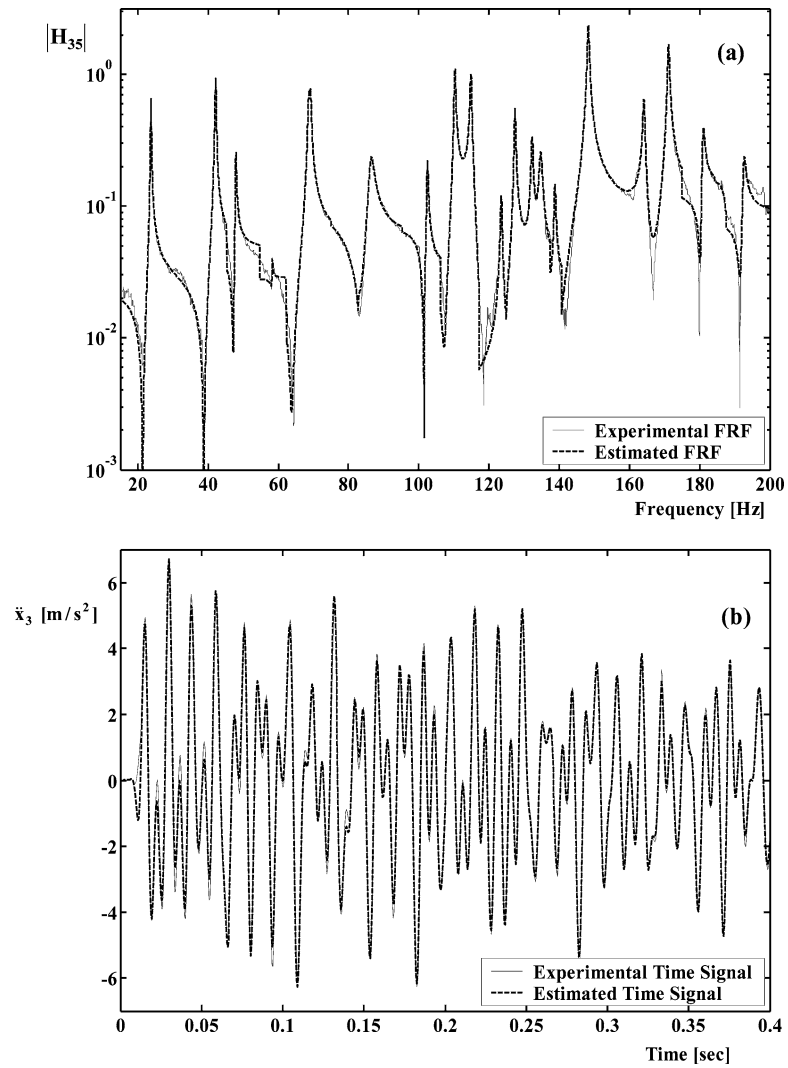

Fig. 9 Comparison of experimentally measured (continuous line) and numerically determined (dashed line) results: (a) for the magnitude of a typical element of the FRF matrix and (b) for the acceleration signal recorded at point 5 of the frame substructure

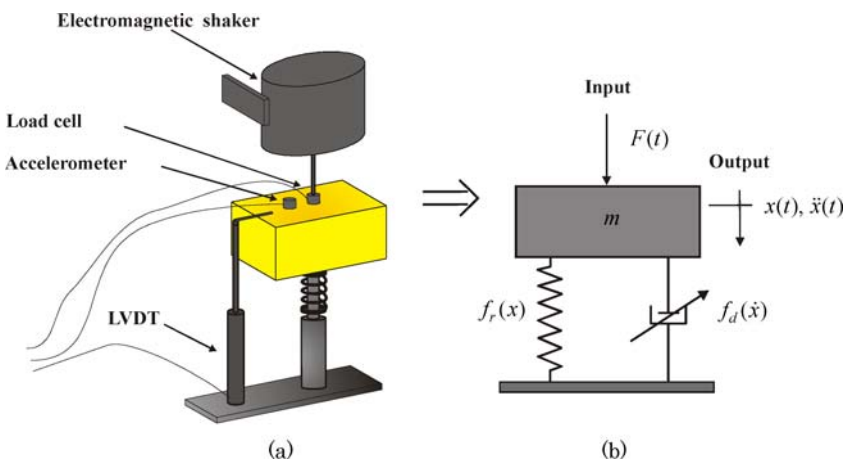

Fig. 10 (a) Experimental set up for measuring the support stiffness and damping parameters. (b) Equivalent mechanical model

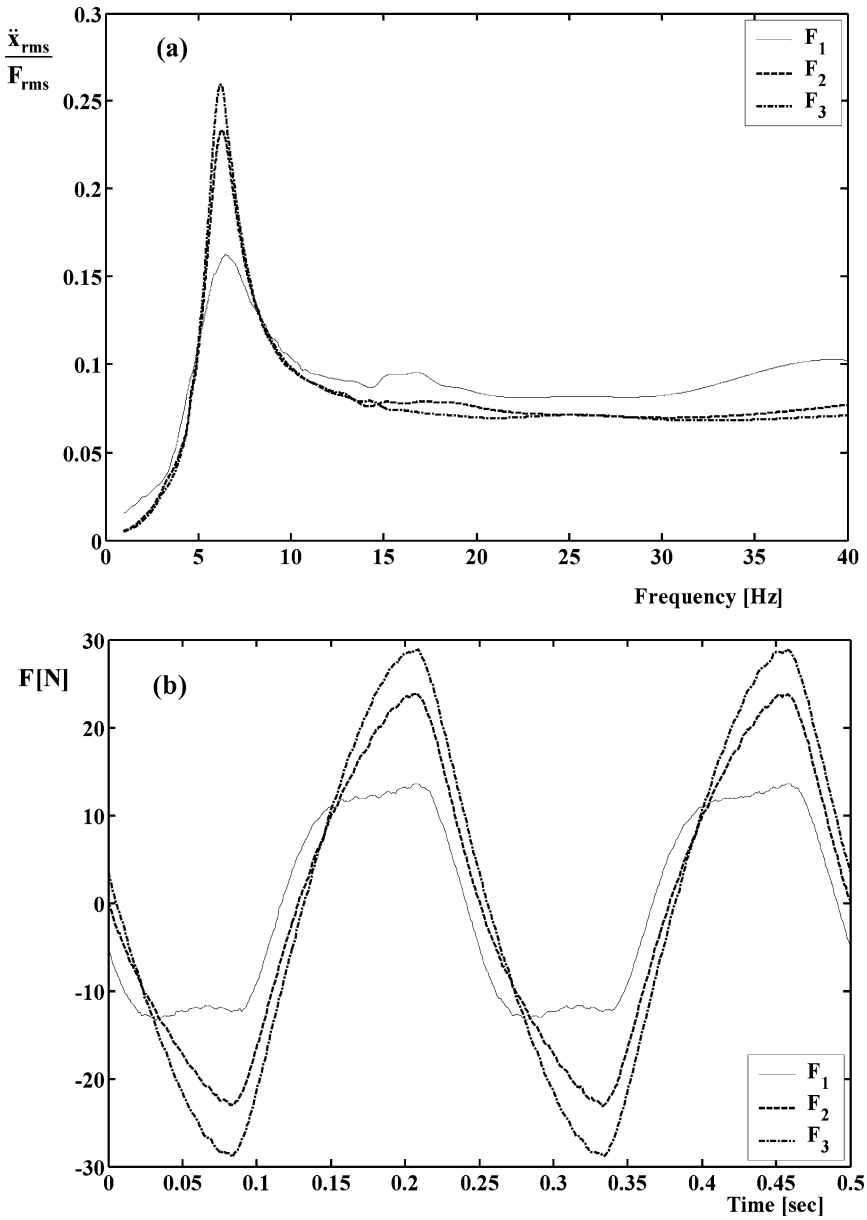

Fig. 11 (a) Transmissibility function of the support system, for three different forcing levels. (b) History of the external force applied with a fundamental harmonic frequency $\omega = 4\,\text{Hz}$

shown in Fig. 11. In particular, Fig. 12a presents the results obtained for k, while Fig. 12b presents the corresponding values for c_1, by assuming linear action of both the spring and the damper. On the other hand, Fig. 12c presents similar results for the damping coefficient c_1, assuming that the restoring and damping forces of the support are expressed by Equations (11) and (12), instead. Obviously, in addition to the nonlinearity already included in the damping force expressed by relation (12), the value of the constant coefficients determined depend to a smaller or larger extend on both the forcing frequency and the forcing amplitude.

The experimental results presented in the last two figures were obtained for the restoring and damping forces of the upper supports. However, similar behavior was also encountered when examining the response as well as the stiffness and damping properties of the lower part of the supports. Based on the optimum values determined for the constant coefficients and the assumed forms of the restoring and damping forces, it was possible to obtain the results shown in Figs. 13a

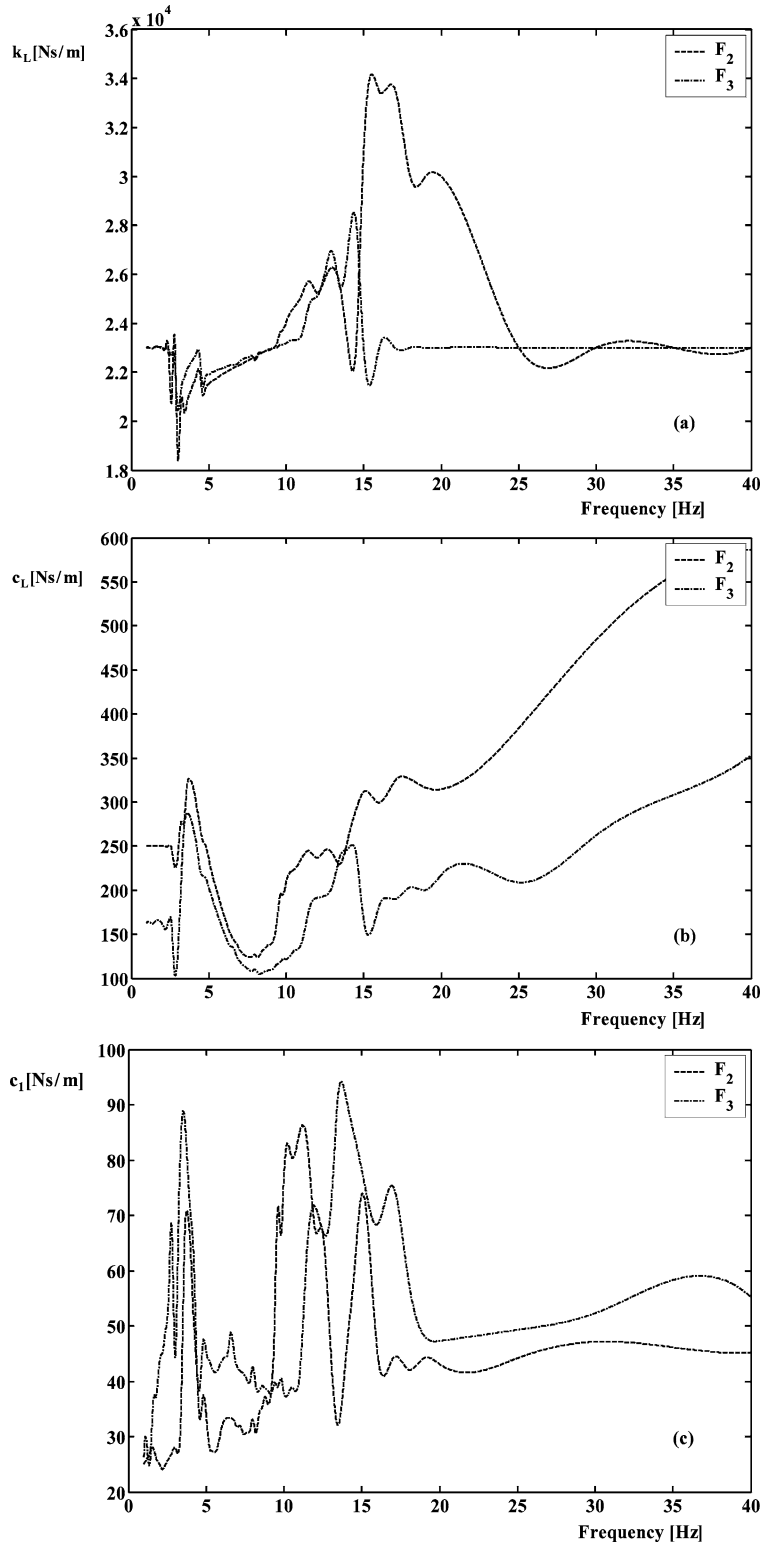

Fig. 12 Stiffness and damping parameters of the upper support units versus forcing frequency, at two forcing levels: (a) stiffness coefficient k_1 and (b) damping coefficient c_1, for linear restoring and damping forces; (c) damping coefficient c_1 for linear restoring force and nonlinear damping force

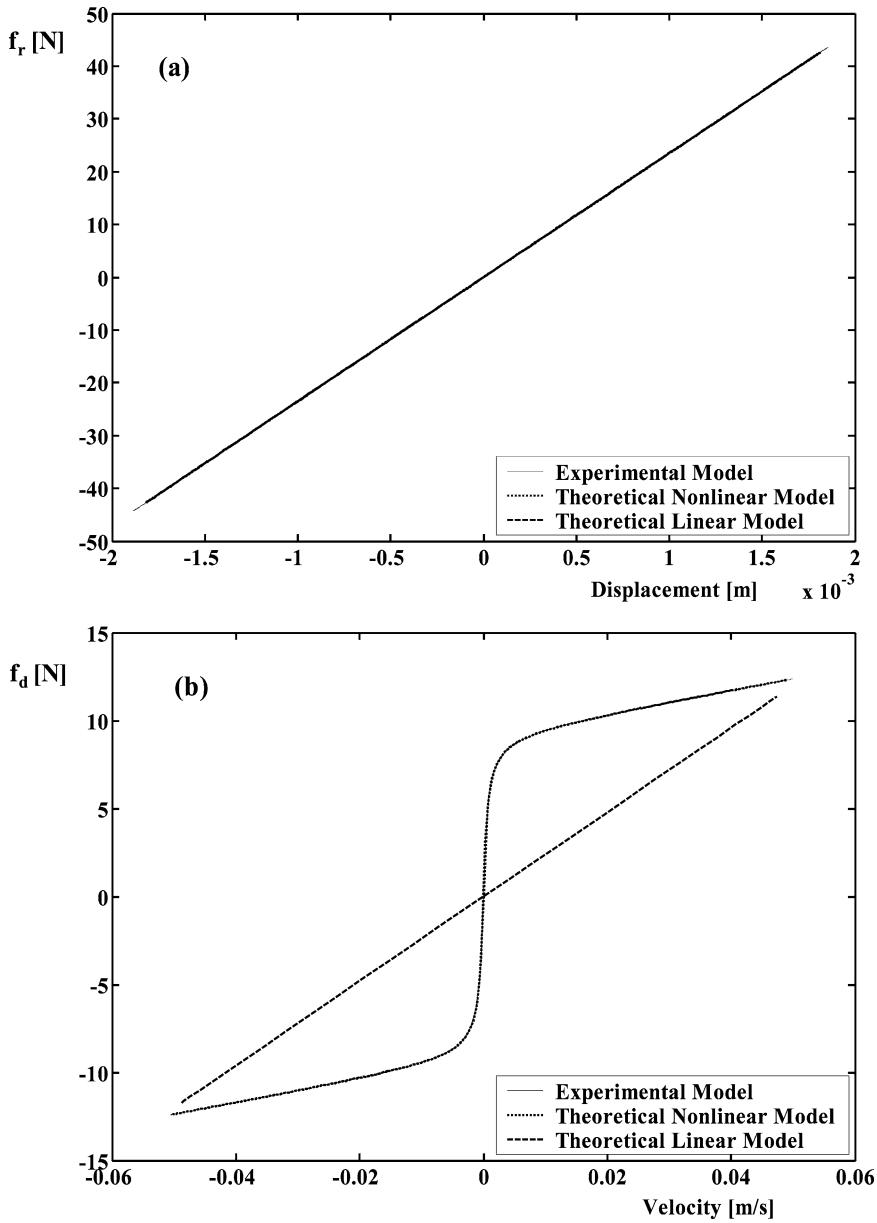

Fig. 13 (a) Restoring force versus displacement and (b) damping force versus velocity, at the upper support units

and 13b, respectively. First, the dashed lines in these figures correspond to results obtained by assuming the classic linear dependence of the restoring force on the displacement and of the damping forces on the velocity of the support unit before integrating the equation of motion corresponding to the single degree of freedom oscillator shown in Fig. 10b. On the other hand, the dotted lines represent similar results, obtained by employing a mechanical model with restoring and damping forces expressed by Equations (11) and (12). Finally, the continuous line represents results obtained by measuring experimentally the signals of $x, \dot{x}$ and employing expressions (11) and (12), again, in order to evaluate the forces f_r and f_d. The comparison of the last two sets of results indicates that sufficient accuracy levels have been achieved by the combined experimental and identification process applied in determining the restoring and damping forces of the supports.

In order to assess in a better way the accuracy of the experimental measurements and the identification process applied in the response predicted, Fig. 14a compares the transmissibility function obtained for one (the intermediate) of the forcing amplitudes employed in obtaining results presented in Fig. 11. First, the results

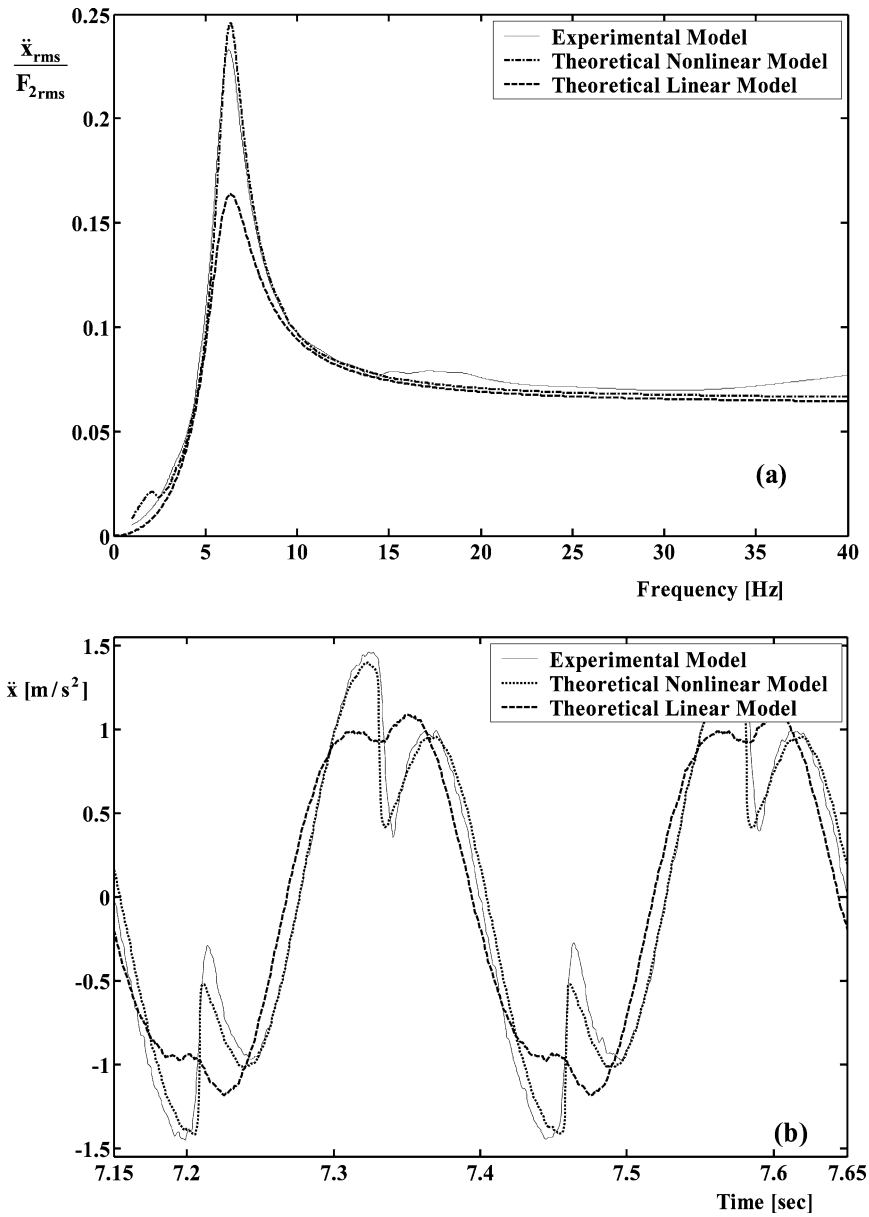

Fig. 14 Comparison of: (a) the acceleration transmissibility function and (b) the acceleration histories obtained experimentally (continuous lines) and numerically (dotted lines for nonlinear and dashed lines for the linear supports), at a fundamental forcing frequency of $\omega = 4\,\text{Hz}$

were obtained by employing the mechanical model shown in Fig. 10b and properties determined experimentally. In particular, numerical results obtained by considering the corresponding linearized support models are represented by the dashed line, while the results obtained by employing relations (11) and (12) are indicated by the dotted line. Finally, the continuous line represents results obtained by direct experimental measurement. On the other hand, Fig. 14b compares the acceleration histories obtained experimentally and numerically at a forcing frequency of $\omega = 4\,\text{Hz}$. The meaning of these lines is the same as in Fig. 14a. Direct comparison demonstrates that the results obtained experimentally (continuous lines) are sufficiently close to those obtained from the numerical model, when using relations (11) and (12) in modeling the restoring and damping forces of the supports and experimentally selected optimum values for the corresponding parameter values (dotted lines). On the other hand, there is a significant deviation between these results and those predicted by the corresponding model where the support units are assumed to exhibit linear restoring and damping forces (dashed lines).

In closing this subsection it is noted that similar levels of agreement were also observed when using other types of excitation, like forcing with periodic or stochastic time dependence. In addition, from all the information presented so far it becomes clear that the complete mechanical system examined in the present section consists of a frame substructure, which can conveniently be modeled by linear characteristics, plus the four supporting substructures, which are characterized by strongly nonlinear action.

4.2. Hybrid modeling with experimental and numerical results

This subsection presents results obtained from hybrid formulations, involving a combination of the dimension reduction methodologies presented in section 2 with experimental results determined for the components of the structural system tested, as explained in the previous subsection. More specifically, the frame substructure of the composite system tested (shown in Fig. 6) was modeled numerically by discretizing it geometrically with the finite element method. In addition, the resulting finite element model was complemented by the damping ratios measured experimentally for the frame substructure. On the other hand, the four supporting substructures were modeled by using the optimum stiffness and damping parameters determined experimentally. In all cases examined, the emphasis was placed on investigating the accuracy of the methodologies applied and in exploring ways to circumvent their shortcomings. Moreover, the dimension of the reduced hybrid models was selected so that their dynamic response is sufficiently accurate for frequencies up to at least 100 Hz.

In many respects, the frequency domain approaches are more convenient to apply than the corresponding time domain methodologies, when adequate experimental information on modal parameters is available [7–11]. For this reason, composite hybrid models of the structure tested were first developed by combining the frequency domain method presented in Section 2.1 with experimental procedures and data, as explained in the previous subsection. First, Fig. 15 presents results obtained by utilizing experimental data, which were determined for both the frame and the supporting substructures, in conjunction with the methodology presented in Section 2.1. Application of this methodology requires the utilization of linear models for both the frame and the supporting substructures. Therefore, the corresponding linearized versions of the restoring and damping forces of all the supporting elements were selected. Moreover, the values of the constant stiffness and damping coefficients were selected to coincide with the corresponding average values determined during the experimental measurements. On the other hand, the transfer functions of the frame substructure were obtained either directly from experimental measurements or numerically, through appropriate manipulation of the equations of motion resulting for the corresponding finite element model.

More specifically, Fig. 15 presents typical results obtained for a diagonal and a non-diagonal element of the FRF function matrix of the composite structure. The FRFs shown are the same with those presented in Fig. 8, which were determined for the frame substructure only. First, an effort was made to perform a comparison between the accuracy obtained by the numerically and the experimentally obtained FRFs for the frame substructure. For this purpose, the continuous lines of Fig. 15 represent results obtained by utilizing the experimentally determined transfer functions of the frame substructure, while the dashed lines correspond to results obtained by utilizing the numerically determined transfer functions of the frame. In both cases, classical damping was assumed, with the damping ratios required for each linear mode selected according to the experimentally determined values. The comparison of the results presented indicates that a sufficient level of agreement has been achieved within the preselected frequency interval of 0–150 Hz. Moreover, for frequencies outside this interval significant deviations start to arise between the experimental and the numerical results.

Although the frequency domain approaches are more fitted to apply in conjunction with experimental procedures, they are also associated with serious drawbacks, due to the fact that they are usually based on linear formulations. As an immediate consequence of this, the results obtained depend heavily on the excitation level applied. For instance, Fig. 16 shows the magnitude of the same FRFs presented in the previous figure, obtained experimentally for the composite system by applying two different excitation levels. In particular, the continuous and dashed lines shown correspond to results obtained for the smaller and the larger forcing amplitude applied, respectively. Obviously, the results shown, together with the results presented in

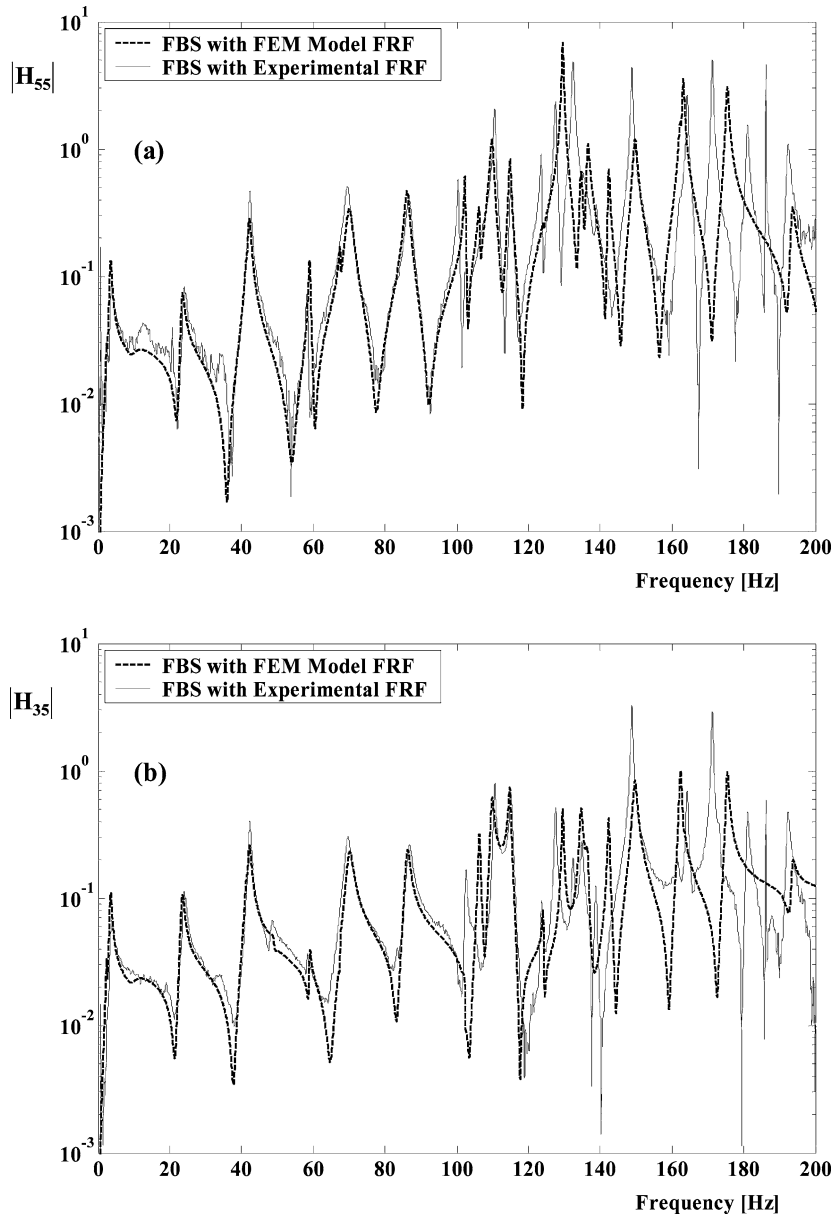

Fig. 15 FRFs of complete system determined by the frequency domain hybrid method: (a) drive point inertance function; (b) transfer inertance function

the previous figure, verify the significant dependence of the response on the excitation level applied, as expected due to the presence of the nonlinearities in the support units.

Since the results obtained through the application of the frequency domain approach depend heavily on the excitation level, the experimental procedure was eventually combined with the time domain hybrid methodology presented in Section 2.2, as explained in the remaining paragraphs of this section. Again, the frame substructure was modeled by the finite element method. However, here the equations of motion were set up in the time domain and include the fully nonlinear characteristics of the suspension dampers. Namely, the equations of motion were finally put into a set of equations like (10). Then, requiring sufficiently accurate response predictions up to 100 Hz led eventually to a reduced model possessing 114 degrees of freedom.

First, Fig. 17a presents a typical acceleration transmissibility function, obtained by experimentally recording both the response of and the excitation applied at the composite system, for two different forcing

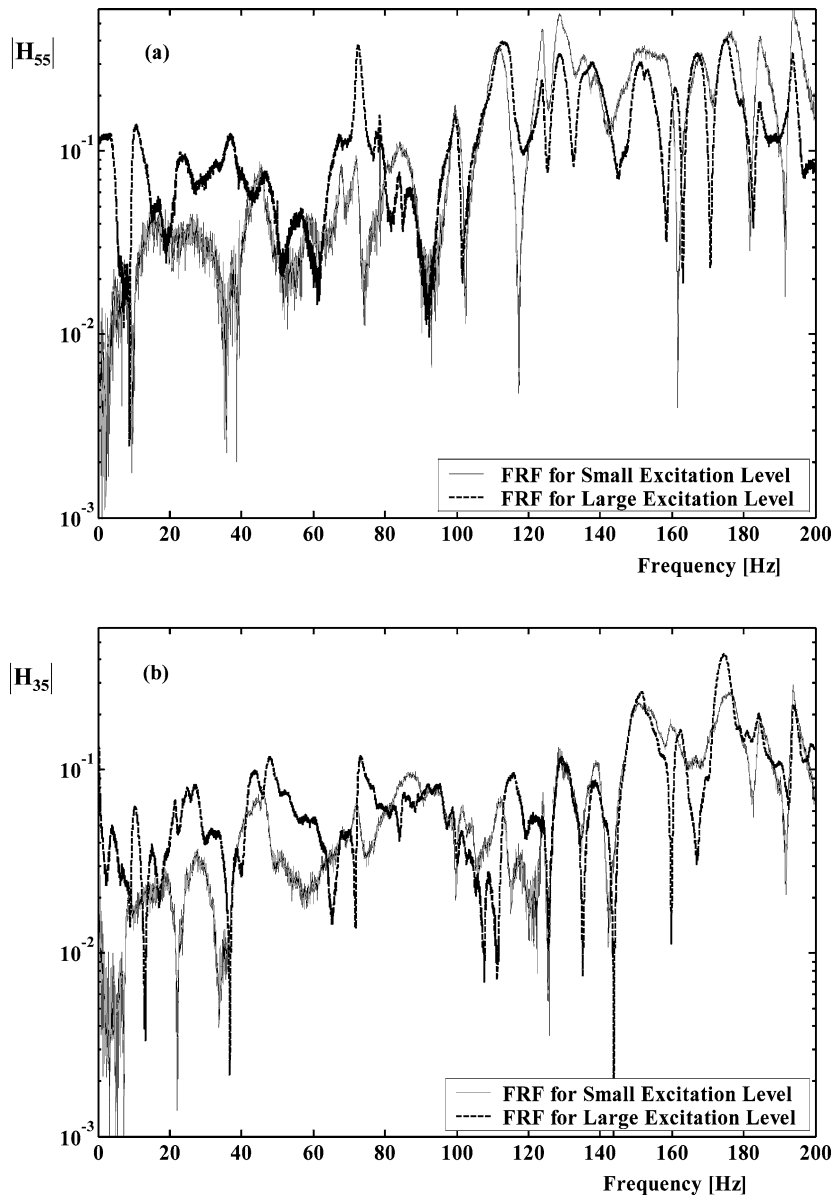

Fig. 16 Comparison of FRFs of the composite system for two different forcing levels: (a) drive point inertance function; (b) transfer inertance function

levels. The continuous and the dashed lines correspond to the smaller and the larger forcing amplitude applied, respectively. This transmissibility function represents the ratio of the root mean square value of the acceleration recorded at point 5 to the root mean square value of the forcing signal measured at the point E of its application (see Fig. 7), for each forcing frequency. Once again, the deviations observed between the two forcing levels reflect the fact that the system examined possesses nonlinear properties. Moreover, neither the applied forcing is actually harmonic, once again, especially within the lower frequency range examined. To illustrate this, Fig. 17b shows two periods of the excitation force applied in each of the same two excitation levels in obtaining the results of Fig. 17a, at a fundamental forcing frequency of $\omega = 3.4$ Hz. The deviation of the forcing signal from the harmonic form becomes larger as the forcing amplitude increases even further.

Finally, Fig. 18a depicts the results of a comparison performed between experimentally determined data with results obtained by applying the time domain hybrid method. In particular, the continuous line represents results obtained for the transmissibility function presented in the previous figure, which was obtained

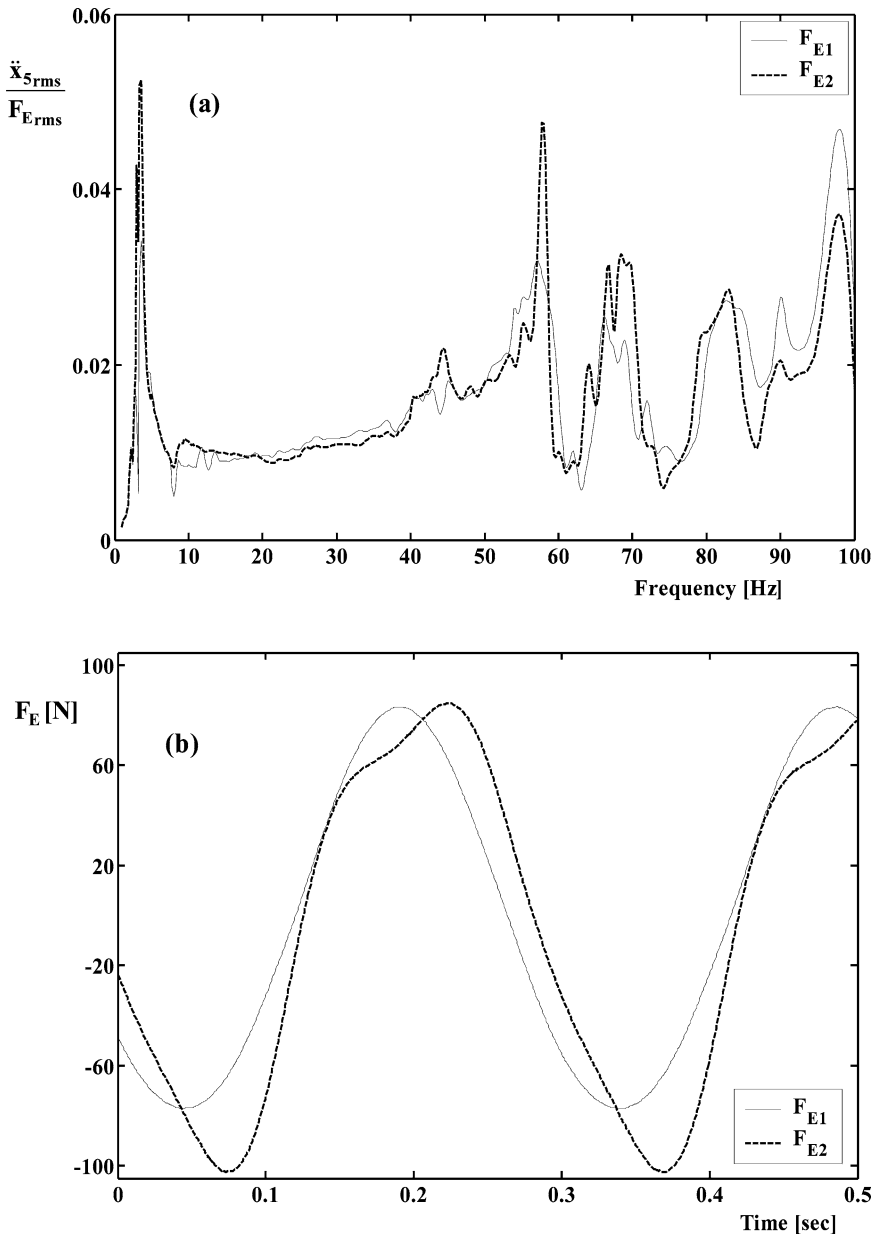

Fig. 17 (a) Acceleration transmissibility function of the complete system, for two different forcing levels. (b) History of the external force applied at point E, with a fundamental frequency $\omega = 3.4$ Hz

by direct experimental measurements corresponding to the larger forcing amplitude. The remaining two curves depict results obtained by applying the hybrid method, employing the finite element model for discretizing the frame substructure and the experimentally determined properties of the supporting substructures. In particular, the results obtained by considering the corresponding linearized support models are represented by the dashed line, while the results obtained by employing relations (11) and (12) are indicated by dots. The forcing imposed at each frequency was identical to the corresponding periodic signal recorded during the experiments at the same frequency. Moreover, due to both the form of the actually applied forcing signal and the support nonlinearities, the system steady state response is in fact periodic instead of harmonic. Direct comparison indicates that there is a significant deviation between the results predicted by the hybrid model when the restoring and damping forces at the support units are assumed to be linear or nonlinear. On the other hand, the results obtained experimentally are now sufficiently close to those obtained from the hybrid

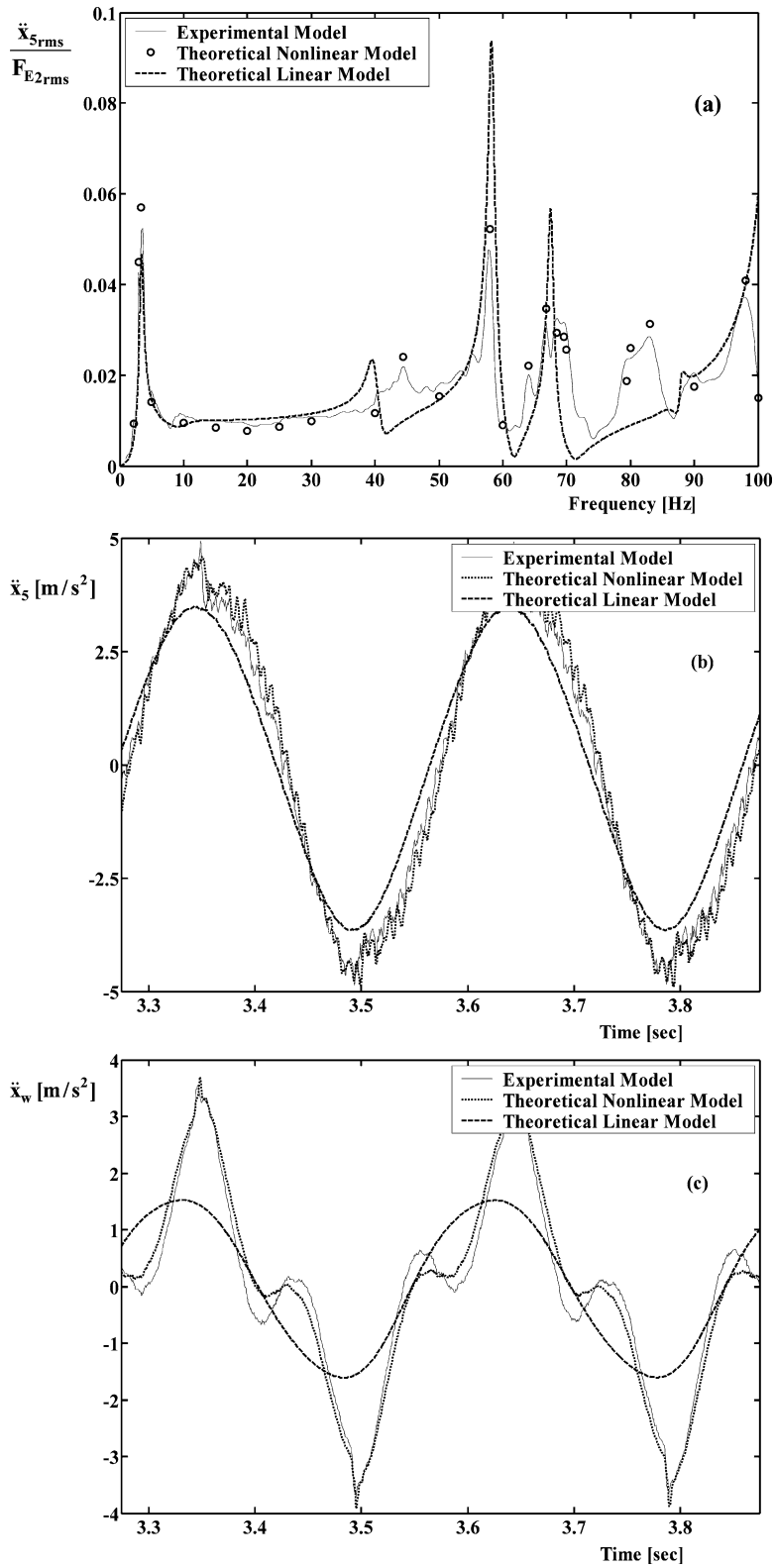

Fig. 18 Comparison of: (a) the acceleration transmissibility function and (b) the acceleration histories obtained experimentally (continuous line) and numerically (dotted line for nonlinear and dashed line for the linear supports), at a fundamental forcing frequency of $\omega = 3.4$ Hz

model, when using relations (11) and (12) in modeling the restoring and damping forces of the supports. To explain this agreement and reinforce this observation even further, Figs. 18b and 18c compare the acceleration histories obtained experimentally and numerically at point 5 and at the front left wheel, respectively, at a forcing frequency of $\omega = 3.4$ Hz. The meaning of the lines is the same as in Fig. 18a. Obviously, the results obtained by employing the time domain hybrid method demonstrate a close agreement between the experimentally measured signals (continuous lines) and the predictions of the hybrid model (dotted lines), when using the nonlinear characteristics of the system. On the other hand, there exist significant differences between these signals and those obtained by applying the hybrid method but with linear properties.

5. Summary

Two hybrid methodologies were applied for determining dynamic response of large scale mechanical systems with linear or nonlinear characteristics, in a systematic and efficient way. According to these methods, some of the system components are modeled numerically, while the parameters of the remaining components are measured experimentally. The basic idea was to start the solution process by first applying a reduction method in either the frequency or the time domain in order to eliminate a substantial number of the original degrees of freedom, so that the reduced model is sufficiently accurate up to a prespecified level of forcing frequencies. Besides the direct computational savings, this reduction in the model dimensions enables the application of powerful numerical and experimental procedures, which are applicable for low order systems only. First, the accuracy and effectiveness of these methodologies was illustrated and confirmed by presenting numerical results for two mechanical models, referring to a gear-pair system and a ground vehicle. Frequency response spectra of several response quantities related to dynamic performance were constructed. Among other things, it was shown that the residual flexibility effects are necessary for improving the model accuracy throughout the low frequency range examined. Then, the same methodologies were applied to a specially designed structure, involving a linear frame component with high modal density and four supporting substructures with nonlinear characteristics, which were identified experimentally. At the beginning, the frequency domain methodology was applied by considering an appropriate linearized model of the support units. However, this led to unacceptably large errors in the response, due to the activation of the support nonlinearities. These difficulties were eventually overcome by applying the time domain hybrid methodology, which led to sufficiently accurate results.

Acknowledgements This research was partially supported by a grant from the General Secretariat of Research and Technology, Greek Ministry of Development, through the PENED 2001 program (01-EΔ-330).

References

1. Rega, G., Alaggio, R., Benedettini, F.: Experimental investigation of the nonlinear response of a hanging cable. Part I: Local analysis. Nonlinear Dyn. **14**, 89–117 (1997)
2. Rega, G., Alaggio, R.: Spatio-temporal dimensionality in the overall complex dynamics of an experimental cable/mass system. Int. J. Solids Struct. **38**, 2049–2068 (2001)
3. Nayfeh, A.H., Balachandran, B.: Applied Nonlinear Dynamics. Wiley, New York (1995)
4. Verros, G., Natsiavas, S.: Ride dynamics of nonlinear vehicle models using component mode synthesis. ASME J. Vib. Acoust. **124**, 427–434 (2002)
5. Nelson, H.D., Meacham, W.L., Fleming, D.P., Kascak, A.F.: Nonlinear analysis of rotor-bearing systems using component mode synthesis. ASME J. Power Eng. **105**, 606–614 (1983)
6. Chen, C.S., Natsiavas, S., Nelson, H.D.: Coupled lateral-torsional vibration of a gear-pair system supported by a squeeze film damper. ASME J. Vib. Acoust. **120**, 860–867 (1998)
7. Cuppens, K., Sas, P., Hermans, L.: Evaluation of FRF based substructuring and modal synthesis technique applied to vehicle FE data. ISMA 2000, Leuven, K.U., Belgium, pp. 1143–1150 (2000)
8. Huizinga, A.T.M.J.M., Campen, D.H. van, Kraker, A. de: Application of hybrid frequency domain substructuring for modelling an automotive engine suspension. ASME J. Vib. Acoust. **119**, 304–310 (1997)
9. Ewins, D.J.: Modal Testing: Theory and Practice. Research Studies Press, Somerset, England (1984)
10. Jetmundsen, B., Bielawa, R.L., Flannelly, W.G.: Generalized frequency domain substructure synthesis. J. Am. Helicopter Soc. **85**, 55–64 (1988)
11. Ren, Y., Beards, C.F.: On substructure synthesis with FRF data. J. Sound Vib. **185**, 845–866 (1995)
12. Craig, Jr., R.R.: Structural Dynamics – An Introduction to Computer Methods. Wiley, New York, (1981)
13. Mottershead, J.E., Friswell, M.I.: Model updating in structural dynamics: A survey. J. Sound Vib. **167**, 347–375 (1993)

14. Fassois, S.D., Eman, K.F., Wu, S.M.: A linear time-domain method for structural dynamics identification. ASME J. Vib. Acoust. **112**, 98–106 (1990)
15. Hac, A., Spanos, P.D.: Time domain method for parameter system identification. ASME J. Vib. Acoust. **112**, 281–287 (1990)
16. Morgan, J.A., Pierre, C., Hulbert, G.M.: Calculation of component mode synthesis matrices from frequency response functions, Part 1: Theory. ASME J. Vib. Acoust. **120**, 503–508 (1998)
17. MSC: MSC/NASTRAN User's Manual–Version 2005. The MacNeal – Schwendler Corporation, Los Angeles, CA (2005)
18. Giagopulos, D.: Parametric modal identification and fault detection in critical safety structures using experimental data. (Ph.D. Thesis). Department of Mechanical Engineering, Aristotle University, Thessaloniki, Greece (2005)
19. Beck, J.L., Jennings, P.C.: Structural identification using linear models and earthquake records. J. Earthq. Eng. Struct. Dyn. **8**, 145–160 (1980)
20. Richardson, M.H., Formenti, D.L.: Global curve fiiting of-frequency response measurements using the rational fraction polynomial method. Third IMAC Conference. Orlando, Florida (1985)
21. Katafygiotis, L.S., Papadimitriou, C., Lam, H.F.: A probabilistic approach to structural model updating. Int. J. Soil Dyn. Earthq. Eng. **17**, 495–507 (1998)
22. Giagopulos, D., Salpistis, C., Natsiavas, S.: Effect of nonlinearities in the identification and fault detection of gear-pair systems. Int. J. Nonlinear Mech. **41**, 213–230 (2006)